CHINESE OPTICS LETTERS

Vol. 19, No. 4 | April 2021

Enhancement of rapid lifetime determination for time-resolved fluorescence imaging in forensic examination

Xin Zhong (钟 鑫)[1,2,†], Xinwei Wang (王新伟)[1,2,3*,†], Liang Sun (孙 亮)[1], and Yan Zhou (周 燕)[1,2,3]

[1] Optoelectronics System Laboratory, Institute of Semiconductors, Chinese Academy of Sciences, Beijing 100083, China

[2] College of Materials Science and Opto-Electronics Technology, University of Chinese Academy of Sciences, Beijing 100049, China

[3] School of Electronic, Electrical and Communication Engineering, University of Chinese Academy of Sciences, Beijing 100049, China

*Corresponding author: wangxinwei@semi.ac.cn

Received June 1, 2020 | Accepted October 9, 2020 | Posted Online December 28, 2020

An enhancement method of rapid lifetime determination is proposed for time-resolved fluorescence imaging to discriminate substances with approximate fluorescence lifetime in forensic examination. In the method, an image-exclusive-OR treatment with filter threshold adaptively chosen is presented to extract the region of interest from dual-gated fluorescence intensity images, and then the fluorescence lifetime image is reconstructed based on the rapid lifetime determination algorithm. Furthermore, a maximum and minimum threshold filtering is developed to automatically realize visualization enhancement of the lifetime image. In proof experiments, compared with traditional fluorescence intensity imaging and rapid lifetime determination method, the proposed method automatically distinguishes altered and obliterated documents written by two brands of highlighters with the same color and close fluorescence lifetime.

Keywords: time-resolved fluorescence imaging; fluorescence lifetime image; visualization enhancement; dual-gated intensity-correlation; forensic examination.

DOI: 10.3788/COL202119.041101

1. Introduction

Imaging techniques have been widely employed in forensic[1] examination, such as infrared spectrum imaging[2–4], fluorescence imaging, and time-resolved fluorescence imaging (TRFI). Different from spectrum imaging[5,6], TRFI discriminates substances based on their different fluorescence lifetimes, which cannot be affected by substance concentration and only depend on their fluorophore molecular environment. Especially, wide-field TRFI has great potential in quickly detecting complex and large fluorescent objects[7–11] and has been successfully applied in overlapped fingerprints revealing[12,13], obliterated documents inspection[14], and gunshot residue determination[15]. For example, Suzuki *et al.*[14] have utilized wide-field TRFI to decipher obliterated documents, and four brands of black inks with similar spectra are separated by TRFI, because different inks have different fluorescence intensities at reasonable delay time and optical gate time. Seah *et al.*[12] have reported that overlapping fingerprints treated with two fluorescent powders can be distinguished by TRFI. In fact, in forensic examination, the traditional TRFI finds the maximum of fluorescence intensity difference between different substances by adjusting reasonable delay time, since different substances have different fluorescence lifetimes. It means that one needs to spend a lot of time to find the suitable delay time as well as optical gate time, while, in judicial document inspection, there are usually a lot of suspicions that need confirmed, and thus rapid detection is desired. Different from fluorescence intensity images, the fluorescence lifetime image directly shows differences in lifetime to distinguish different substances. Therefore, in this paper, we introduce rapid fluorescence lifetime determination (RLD) to quickly obtain lifetime maps in forensic examination. For the wide-field time-domain fluorescence lifetime imaging, the RLD method only needs two time-resolved fluorescence intensity images to satisfy transient fluorescence lifetime imaging[16–19], and it is more suitable for observing active objects or a larger number of objects than other methods. However, when interference noise is high, the RLD method has image quality degradation and indistinguishability, especially when the lifetime is similar. To solve the problem, this paper proposes an enhanced RLD (ERLD) imaging method based on dual-gated intensity correlation to enhance the discrimination of fluorescent substances and make them easier to be quickly distinguished by human eyes. Different from the

method[20,21] of improving calculation accuracy and analyzing calculation error, the proposed method in this paper is to improve the contrast of lifetime images.

2. Enhanced Rapid Lifetime Determination Imaging Method

As shown in Fig. 1(a), a typical wide-field TRFI system consists of a pulsed laser, a gated optical intensifier (GOI), a charge-coupled device (CCD) camera, and timing control unit (TCU). The TCU controls the GOI gate time, CCD exposure time, and the laser pulse width, simultaneously. The ERLD method is based on a wide-field TRFI system, and its principle is illustrated in Fig. 1. A UV laser with picosecond-scaled pulse width is used to generate excitation light. The output laser irradiates the fluorescence substances. The excited fluorescence is generated and reflected to the GOI. This nanosecond-scaled GOI is operated at the same repetition rate as the laser. GOI is coupled to the CCD camera. TCU generates delay time to trigger GOI and CCD to grasp TRFI images.

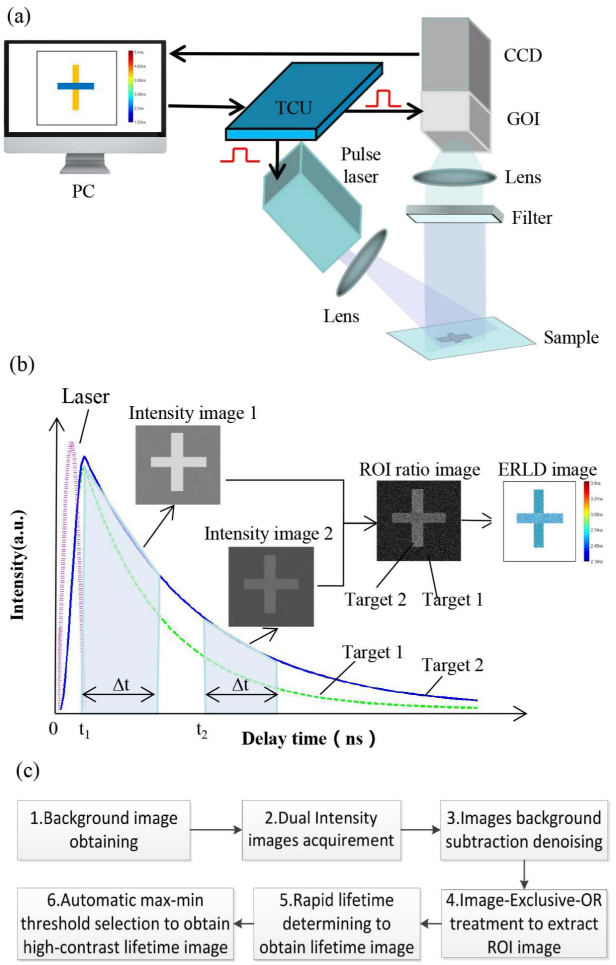

Fig. 1. (a) Schematic diagram of the wide-field TRFI system, (b) principle of the ERLD method, and (c) process diagram of the ERLD method.

In Fig. 1(a), the given target of the cross letter "+" is written on the paper. The " | " and "−" are written by different highlighters. The interference of fluorescence substances and the background noise lead to low contrast time-resolved intensity images. Here, the ERLD method is proposed, and it involves six steps, as shown in Fig. 1(c).

In Fig. 1(b), two time-resolved fluorescence intensity images are grasped at different delay times. The gate time of two intensity images is equal as Δt. When there are different substances, the single intensity image for multiple substances is given as

$$I(t) = \sum_{k=1}^{M} I_{\text{target},k}(t) + I_{\text{environment noise}} + I_{\text{system noise}}, \quad (1)$$

where M is the number of fluorescence substances, I_{target} is the target signal, $I_{\text{environment noise}}$ represents the environmental noise considered as Poisson noise[11], and $I_{\text{system noise}}$ is the system noise caused by all devices in the system and considered as Gaussian noise.

Two intensity images are processed in six steps to finally obtain contrast enhanced lifetime images, as shown in Fig. 1(c). The detailed instructions of the six steps are as follows.

The first step is background image acquisition at no incident light. $I_{\text{background}}$ obtains the intensity of environmental noise and system noise. The second step is to acquire two intensity images at two different delay times. The third step is the subtraction of background to remove the environmental noise and system noise and generate a new intensity image $I_{\text{new}}(t)$:

$$I_{\text{new}}(t) = I(t) - I_{\text{background}} = \sum_{k=1}^{M} I_{\text{target},k}(t) + I_{\text{residual noise}}, \quad (2)$$

where $I_{\text{residual noise}}$ is the residual interference noise that cannot be eliminated by background subtraction denoising. It needs to be further eliminated to improve the contrast of the image.

The fourth step is to further suppress the noise. As shown in Eq. (3), there is effective information and residual noise in $I_{\text{new}}(t)$. It leads to low contrast images. Hence, the image-exclusive-OR treatment is presented to extract the region of interest (ROI) from the two new images $I_{\text{new}}(t_1)$ and $I_{\text{new}}(t_2)$. Then, the ratio image of the two intensity images can be obtained as

$$R_{i,j} = \begin{cases} 0 & I_{\text{new}}(t_1)_{i,j} < I_{\text{thres}} \text{ or } I_{\text{new}}(t_2)_{i,j} < I_{\text{thres}} \\ R_{\text{ratio}} = \frac{I_{\text{new}}(t_1)_{i,j}}{I_{\text{new}}(t_2)_{i,j}} & I_{\text{new}}(t_1)_{i,j} > I_{\text{thres}} \text{ and } I_{\text{new}}(t_2)_{i,j} > I_{\text{thres}} \end{cases}, \quad (3)$$

where I_{thres} is the value of the filter threshold and R_{ratio} is the ratio image of the ROIs in $I_{\text{new}}(t_1)$ and $I_{\text{new}}(t_2)$.

When the gray value of the intensity image at the delay time t_1 or t_2 is smaller than the filter threshold, the value of the corresponding pixel is set to zero. In order to evaluate the effect of contrast enhancement, the image variance is applied as

$$V = \frac{\sum (R_{i,j} - \bar{R})^2}{N}, \tag{4}$$

where N is the number of pixels in an image, and $\bar{R}$ is the mean gray value of all pixels. Theoretically, the larger variance means the higher image contrast, and thus the filter threshold can be selected by finding the maximum of V.

The fifth step is the lifetime image obtained by Eq. (5):

$$\tau_{i,j} = \frac{t_2 - t_1}{\ln R_{i,j}}. \tag{5}$$

To improve the lifetime image contrast, the gray contrast enhancement is used as the sixth step. As shown in Eq. (6), when the gray value of $\tau_{i,j}$ is smaller than the minimum threshold of $\tau_{\min}$ and greater than the maximum threshold of $\tau_{\max}$, it is set to NaN, and otherwise the grayscale stretching is used:

$$\tau_{\text{new}(i,j)} = \begin{cases} \text{NaN} & \tau_{i,j} \le \tau_{\min} \\ (2^B - 1)\frac{\tau_{i,j} - \tau_{\min}}{\tau_{\max} - \tau_{\min}} & \tau_{\min} < \tau_{i,j} < \tau_{\max} \\ \text{NaN} & \tau_{i,j} \ge \tau_{\max} \end{cases}, \tag{6}$$

where B is the gray bit depth, and τ_{new} is the stretched image. After the processing of Eq. (6), the invalid pixels are removed, and the image gray histogram is stretched.

Due to the fluorescence delay function, $I(t_1)$ should be larger than $I(t_2)$. Hence, $\tau_{\min}$ is larger than zero. $\tau_{\min}$ can be automatically set to the minimum non-zero value. $\tau_{\max}$ is selected based on the contrast of the lifetime image. The contrast of the enhanced lifetime image is expressed by the effective variance V_{eff} as

$$V_{\text{eff}} = \eta \frac{\sum (\tau_{\text{neweff}(i,j)} - \bar{\tau}_{\text{neweff}})^2}{N_{\text{eff}}}, \tag{7}$$

where N_{eff} is the sum of the effective pixels of the enhanced lifetime image, τ_{neweff} is the effective pixels of the lifetime image, $\bar{\tau}_{\text{neweff}}$ is the mean of the effective pixels, and η is the effective pixels descriptor of the enhanced image to evaluate N_{eff} and is defined as $\eta = N_{\text{eff}}/N$, where N is the number of all pixels. The significance of parameter η is to calculate the proportion of effective pixels in all pixels. The value of $\tau_{\max}$ can be chosen by finding the maximum of V_{eff}.

After all six steps have been completed, pseudo-color coding is used to improve the visibility of the enhanced image, and a fluorescence lifetime image is finally obtained. The maximum and minimum limits of the colorbar of the pseudo-color image are $\tau_{\max}$ and $\tau_{\min}$, respectively.

In addition, when the environment and the test objects are unchanged, the filter threshold and maximum and minimum threshold values can also be fixed after being automatically obtained. It is not necessary to find the thresholds again.

The ERLD method enhances the visualization of lifetime fluorescence imaging for finely distinguishing fine detection. To prove the feasibility of the proposed method, verification experiments are conducted. The RLD method is a classic fluorescence lifetime algorithm. ERLD and RLD methods are both using two time-resolved images, but our method gives priority to suppress noise and automatically improve the contrast of the lifetime image. In order to illustrate the difference, we introduce the traditional TRFI and RLD methods to compare the image contrast.

3. Experiment and Results

In experiments, a wide-field TRFI system has been established. The narrow-pulse UV laser is a PicoQuant PDL800-B type with the laser pulse width of 50 ps at the wavelength of 375 nm. The gated sensor is a PI-MAX4 intensified CCD (ICCD) from Princeton Instruments with a minimum optical gate width of 3 ns and 1024×1024 pixels. A field-programmable gate array (FPGA) is used as a time control unit to synchronize the pulsed laser and the gated ICCD. A 400 nm cut-off filter is used in front of the lens to block the reflected UV light.

To prove the proposed method, we choose two bands of highlighters in the same color, and they cannot be distinguished by the naked eye. The spectral information of GUANGBO and M&G is 520 nm and 527 nm, respectively. Different brands of highlighters contain different proportions of chemicals and, thus, have different fluorescence lifetimes. The paper we used also has fluorescence characteristics, and the fluorescence of papers affects the fluorescence image quality.

In Fig. 2(a), two highlighters of GUANGBO and M&G are marked on the paper. The difference in fluorescence lifetime

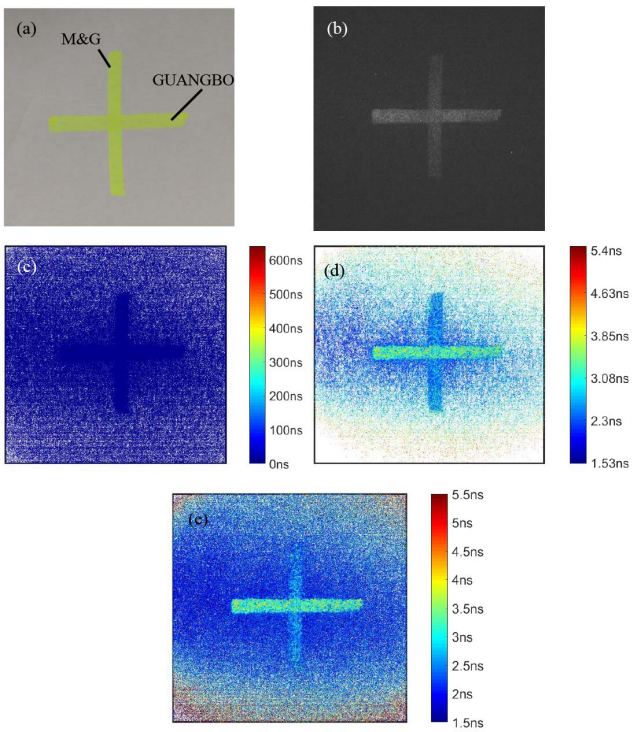

Fig. 2. Experimental results of cross letter written by M&G and GUANGBO under different methods: (a) target picture, (b) intensity image, (c) traditional RLD image, (d) ERLD image, and (e) manual RLD image.

between GUANGBO and M&G is small. Figures 2(b) and 2(c) are a TRFI intensity image and a traditional RLD image, respectively. One cannot distinguish the deference of the marks clearly. Especially in Fig. 2(c), the effective information is completely covered by an invalid value. Because of the influence of interference noise, there is a very large deviation in the calculated lifetime image obtained by the traditional RLD method. In comparison, the difference of highlighters is revealed in Fig. 2(d) through the ERLD method. The horizontal and the vertical marks are marked with different colors and can be better distinguished by the naked eye. According to Fig. 2(d) obtained by the ERLD method, the maximum and minimum limits of the colorbar scale are manually selected for Fig. 2(c), and the result is shown in Fig. 2(e). It also obtains high-contrast images, but the contrast of the image is worse than that of the ERLD image. It is mainly because the image-exclusive-OR treatment of ERLD can effectively remove interference noise. In the experiment, the delay time is the time gap between the incident laser pulse and the optical gate pulse. In Fig. 2(b), the delay time is 7 ns, and the optical gate time is 5 ns. In Figs. 2(c) and 2(d), they have the same first delay time of $t_1 = 7$ ns and the same second delay time of $t_2 = 14$ ns, and the optical gate time is 5 ns.

Figure 3 shows the variance changes with the filter threshold and maximum and minimum thresholds. When the filter threshold increases, the image variance changes dramatically in Fig. 3(a), and the fluctuation is due to the interference signal. Figure 3 demonstrates that the filter threshold and maximum threshold are chosen when the image variances are the maximum, and the minimum threshold is set to the minimum non-zero value.

To prove that the proposed method is also available in obliterated document examination, Fig. 4(a) is a letter A written by M&G and then covered by GUANGBO to make it invisible. The ERLD image of Fig. 4(c) can clearly show the letter A from the mask due to different lifetimes, although the mark is slightly different in intensity. The manual RLD image of Fig. 4(d) also has high contrast by setting the same maximum and minimum limits of the colorbar according to Fig. 4(c). In other words, if there is no reference of the colorbar from Fig. 4(c), one needs to manually choose the colorbar scale, and it is not convenient in practical applications of forensic examination. Furthermore, because there is no image-exclusive-OR treatment processing, the residual interference noise exists in Fig. 4(d). In Fig. 4(b), the delay time is 14 ns, and the optical gate time is 5 ns. In Figs. 4(c) and 4(d), they have the same first delay time of $t_1 = 14$ ns and the same second delay time of $t_2 = 21$ ns, and the optical gate time is 5 ns.

To evaluate the proposed method, the contrasts of global images are given, as shown in Table 1. The contrast of the global image is used to assess the quality of the whole image. The contrast of the global image is defined as the root mean square deviation of the effective pixels' gray values from the mean pixel gray values of the image, divided by the global image's mean gray values[22].

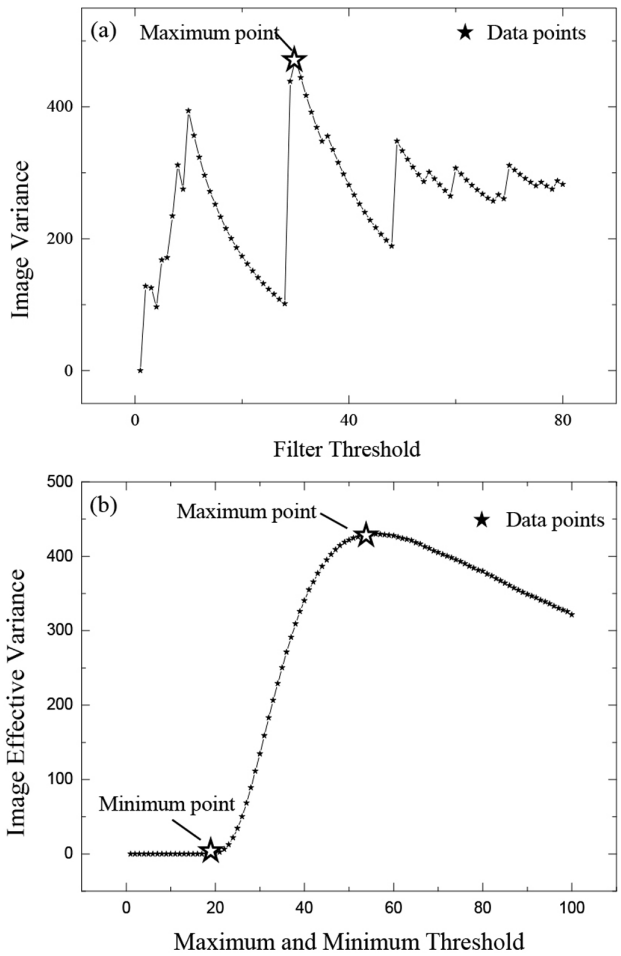

Fig. 3. Variance distribution with (a) filter threshold and (b) maximum and minimum thresholds in ERLD images.

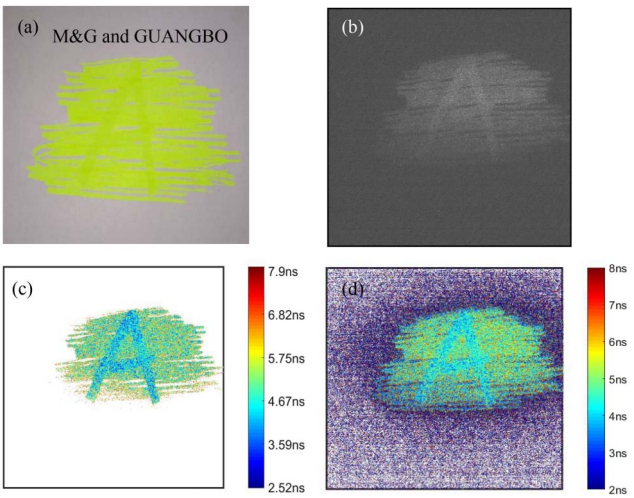

Fig. 4. Results of obliterated document: (a) target picture, (b) intensity image, (c) ERLD image, and (d) manual RLD image.

Table 1. Different Contrast of Three Methods.

	Intensity Image	ERLD Image	Manual RLD Image
Fig. 2	0.0475	1.4580	0.8485
Fig. 4	0.0667	2.2987	0.5586

4. Conclusion

Multi-fluorescence overlap is difficult to distinguish in wide-field TRFI for forensic casework. This paper has proposed an ERLD method to remove environmental noise, system noise, and residual interference noise. The proposed method enhances fluorescence lifetime image contrast and improves the visualization performance of TRFI. Compared with traditional TRFI and RLD methods, the proposed method can maintain a high contrast and automatically make the lifetime image easier to be observed. Moreover, the experiment results show that the ERLD method can automatically select maximum and minimum thresholds to remove unwanted noise and improve lifetime image contrast by grayscale stretching. Even when the difference in fluorescence lifetime is small, the proposed method can still distinguish different fluorescent substances.

Acknowledgement

This work was supported by the National Natural Science Foundation of China (NSFC) (No. U1736101) and the Youth Innovation Promotion Association CAS (No. 2017155).

†The authors contributed equally to this work.

References

1. W. Wei, L. Huang, X. Zhu, L. Ling, K. Guo, and H. Huang, "Application of reflectance transformation imaging for the display of handwriting traces," Chin. Opt. Lett. **17**, 111101 (2019).
2. T. Liu, H. Liu, Y. Li, Z. Chen, Z. Zhang, and S. Liu, "Flexible FTIR spectral imaging enhancement for industrial robot infrared vision sensing," IEEE Trans. Ind. Inform. **16**, 544 (2020).
3. T. Liu, H. Liu, Y. Li, Z. Zhang, and S. Liu, "Efficient blind signal reconstruction with wavelet transforms regularization for educational robot infrared vision sensing," IEEE Trans. Ind. Inform. **24**, 384 (2019).
4. T. Liu, H. Liu, Z. Chen, and A. M. Lesgold, "Fast blind instrument function estimation method for industrial infrared spectrometers," IEEE Trans. Ind. Inform. **14**, 5268 (2018).
5. Z. Zhang, J. Chang, H. Ren, K. Fan, and D. Li, "Snapshot imaging spectrometer based on a microlens array," Chin. Opt. Lett. **17**, 011101 (2019).
6. N. Zhao, J. Li, Q. Ma, L. Guo, and Q. Zhang, "Periphery excitation of laser-induced CN fluorescence in plasma using laser-induced breakdown spectroscopy for carbon detection," Chin. Opt. Lett. **18**, 083001 (2020).
7. Y. Chen and R. M. Clegg, "Fluorescence lifetime-resolved imaging," Photosynth. Res. **102**, 143 (2009).
8. R. Cubeddu, D. Comelli, C. D' Andrea, P. Taroni, and G. Valentini, "Time-resolved fluorescence imaging in biology and medicine," J. Phys. D **35**, R61 (2002).
9. D. Comelli, C. D' Andrea, G. Valentini, R. Cubeddu, and C. Colombo, "Fluorescence lifetime imaging and spectroscopy as tools for nondestructive analysis of works of art," Appl. Opt. **43**, 2175 (2004).
10. Z. Petrášek, H. J. Eckert, and K. Kemnitz, "Wide-field photon counting fluorescence lifetime imaging microscopy: application to photosynthesizing systems," Photosynth. Res. **102**, 157 (2009).
11. K. C. Benny Lee, J. Siegel, S. E. D. Webb, S. Leveque-Fort, M. J. Cole, R. Jones, K. Dowling, M. J. Lever, and P. M. W. French, "Application of the stretched exponential function to fluorescence lifetime imaging," Biophys. J. **81**, 1265 (2001).
12. L. K. Seah, U. S. Dinish, S. K. Ong, Z. X. Chao, and V. M. Murukeshan, "Time-resolved imaging of latent fingerprints with nanosecond resolution," Opt. Laser Technol. **36**, 371 (2004).
13. L. K. Seah, P. Wang, V. M. Murukeshan, and Z. X. Chao, "Application of fluorescence lifetime imaging (FLIM) in latent finger mark detection," Forensic. Sci. Int. **160**, 109 (2006).
14. M. Suzuki, N. Akiba, K. Kurosawa, K. Kuroki, Y. Akao, and Y. Higashikawa, "Wide-field time-resolved luminescence imaging and spectroscopy to decipher obliterated documents in forensic science," Opt. Eng. **55**, 014101 (2016).
15. D. K. Bird, K. M. Agg, N. W. Barnett, and T. A. Smith, "Time-resolved fluorescence microscopy of gunshot residue: an application to forensic science," J. Microsc. **226**, 18 (2007).
16. A. V. Agronskaia, L. Tertoolen, and H. C. Gerritsen, "High frame rate fluorescence lifetime imaging," J. Phys. D **36**, 1655 (2003).
17. D. S. Elson, I. Munro, J. Requejo-Isidro, J. Mcginty, C. Dunsby, N. Galletly, G. W. Stamp, M. A. A. Neil, M. J. Lever, P. A. Kellett, A. Dymoke-Bradshaw, J. Hares, and P. M. W. French, "Real-time time-domain fluorescence lifetime imaging including single-shot acquisition with a segmented optical image intensifier," New J. Phys. **6**, 180 (2004).
18. D. M. Grant, J. McGinty, E. J. McGhee, T. D. Bunney, D. M. Owen, C. B. Talbot, W. Zhang, S. Kumar, I. Munro, P. M. P. Lanigan, G. T. Kennedy, C. Dunsby, A. I. Magee, P. Courtney, M. Katan, M. A. A. Neil, and P. M. W. French, "High speed optically sectioned fluorescence lifetime imaging permits study of live cell signaling events," Opt. Express **15**, 15656 (2007).
19. C. W. Chang and M. A. Mycek, "Enhancing precision in time-domain fluorescence lifetime imaging," J. Biomed. Opt. **15**, 056013 (2010).
20. K. K. Sharman, A. Periasamy, H. Ashworth, J. N. Demas, and N. H. Snow, "Error analysis of the rapid lifetime determination method for double-exponential decays and new windowing schemes," Anal. Chem. **71**, 947 (1999).
21. D. D. Li, S. Ameer-Beg, J. Arlt, D. Tyndall, R. Walker, D. R. Matthews, V. Visitkul, J. Richardson, and R. K. Henderson, "Time-domain fluorescence lifetime imaging techniques suitable for solid-state imaging sensor arrays," Sensors **12**, 5650 (2012).
22. M. Pavel, G. Sperling, T. RiedI, and A. Vanderbeek, "Limits of visual communication: the effect of signal-to-noise ratio on the intelligibility of American Sign Language," J. Opt. Soc. Am. A **4**, 2355 (1988).